Diastereospecific synthesis and amphiphilic properties of new alkyl β-D-fructopyranosides

Vincent Ferrières,[a] Thierry Benvegnu,[a] Martine Lefeuvre,[a] Daniel Plusquellec,*[a] Grahame Mackenzie,[b] Marcus J. Watson,[b] Julie A. Haley,[b] John W. Goodby,*[b] Ron Pindak[c] and Mary K. Durbin[c]†

[a] *Laboratoire de Chimie Organique et des Substances Naturelles, associé au CNRS, Ecole Nationale Supérieure de Chime de Rennes, Avenue du Général Leclerc, 35700 Rennes, France*
[b] *The Department of Chemistry, The Faculty of Science and the Environment, The University of Hull, Hull, UK HU6 7RX*
[c] *Bell Laboratories, Lucent Technologies, 600 Mountain Avenue, Murray Hill, NJ 07974, USA*

Received (in Cambridge) 6th January 1999, Accepted 19th March 1999

In this article we describe a novel one step stereocontrolled synthesis of alkyl 1-*O*-β-D-fructopyranosides from totally unprotected D-fructose. In order to avoid oligomerization of D-fructose the reactions were performed in heterogeneous media. Thus, long chain alcohols, as acceptors, were treated with D-fructose in the presence of iron(III) chloride as the promoter to give the alkyl substituted products in yields of approximately 30%. The materials produced were found to self-organise and form liquid crystal mesophases. One of the thermotropic phases exhibited by this family of compounds was found to be atypical of liquid crystal modifications normally exhibited by glycolipids. The structure of this phase was investigated by a wide variety of techniques, and sufficient evidence was gained to indicate that it is novel. A variety of possible arrangements of the molecules in the self-organised state is given based on the preliminary data.

1 Introduction

D-Fructose is one of the most naturally abundant carbohydrates. It appears generally as a β-furanosyl residue in sucrose or in plant and bacterial polysaccharides.[1] Inulins and levans, which provide respective examples of β-(1,2)- and β-(2,6)-glycosidic linkages between D-fructofuranose moieties, possess interesting biofunctional properties and are involved, for instance, in defence mechanisms against microorganisms or as food reservoirs.[2] As a consequence of their biological importance, various enzymatic and chemical methods have been proposed for the synthesis of D-fructofuranosyl derivatives.

Although substituted D-glucoses can be converted into the corresponding D-fructoses by means of an appropriate glucose isomerase,[3] sucrose, as a D-fructofuranosyl donor, appears also to be a good substrate for an invertase in the preparation of alkyl β-D-fructofuranosides.[4] On the other hand, chemical approaches to substituted D-fructoses generally require the availability of 1,3,4,6-tetra-*O*-protected D-fructofuranoses[5–7] as starting materials. For example, under Mitsunobu conditions, the corresponding acetylated compound yields the expected alkyl and aryl derivatives.[7] However, the synthesis of more complex targets requires more efficient methodologies. Kotchetkov and co-workers[8] first investigated D-fructofuranosyl thiorthoesters and thiofructosides as donors. The latter were also used by Wu and Li[9] and by Oscarson and Krog-Jensen[10] to synthesize 2,3-*trans*-D-fructofuranosides. In combination with the internal aglycon delivery approach,[11] thiofructosides afforded the opposite anomer, *i.e.* β-D-fructofuranosides.[12] Furthermore, Schmidt *et al.*[13] studied the reactivity of anomeric D-fructofuranosyl phosphites towards various glucose and lactose acceptors. However, few examples are known concerning the specific syntheses of pyranosides derived from fructose, and more generally from ketoses. Addition of glycosyl acceptors to *exo*-cyclic epoxides, *exo*-methylene carbohydrates and pyranolactones was investigated by several research groups.[14–16] Nevertheless, syntheses of D-fructopyranosides starting from D-fructose are less well-developed, probably because fructosyl donors in the pyranosyl configuration are available only with difficulty.[17] Actually, unprotected D-fructose in polar solvents, such as dimethyl sulfoxide, pyridine and water, produces the four cyclic forms, *i.e.*, anomeric pairs of both pyranoses and furanoses, along with the open-chain ketose form, making tautomerism fixation considerably more difficult.[17,18] As a result, glycosidation of fructose under Fischer conditions[19] generally affords a mixture of the four fructosides and possibly the acetal derivative.[20]

In the course of our studies on selective modifications of partially or fully unprotected carbohydrates,[21] the D-fructosylation of long chain alcohols in acidic media was reinvestigated. Thus, the materials that were targeted for synthesis had template structures consisting of a polar head connected to a hydrophobic chain *via* a defined glycosidic linkage, see Fig. 1. Generally, glycosidic amphiphiles readily self-assemble and self-organise to give a variety of thermotropic and lyotropic liquid crystal phases, and they find applications as surfactants or specialised non-ionic detergents, especially for the solubilisation and the extraction of membrane proteins.[22] In this article we describe, in full, the stereospecific synthesis of a family of alkyl β-D-fructopyranosides **I** (compounds **10**–**16**, Scheme 1) and we give, in detail, results concerning their unique self-organising properties.

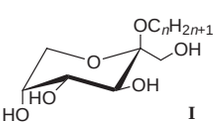

I

Fig. 1 General structure of the fructopyranosides studied.

† Present address: SPAWAR System Center, Code D36, 49590 Lassing Dr, San Diego, CA 92152, USA.

Table 1 Synthesis and analytical data of compounds **10**–**16**

ROH (1.5 equiv.)	Product	Yield (%)	$[\alpha]_D^{20}$ (c = 1, 1,4-dioxane)	Formulae	Anal. Calcd. C(%)	Anal. Calcd. H(%)	Anal. Found C(%)	Anal. Found H(%)
2: n-$C_6H_{13}OH$	**10**	31	−105	$C_{12}H_{24}O_6$	54.53	9.15	54.87	9.42
3: n-$C_8H_{17}OH$	**11**	33	−102	$C_{14}H_{28}O_6$	57.51	9.65	57.33	9.71
4: n-$C_{10}H_{21}OH$	**12**	33	−97	$C_{16}H_{32}O_6$	59.97	10.06	60.00	10.32
5: n-$C_{12}H_{25}OH$	**13**	35	−83	$C_{18}H_{36}O_6$	62.04	10.41	62.10	10.72
6: n-$C_{14}H_{29}OH$	**14**	35	−78	$C_{20}H_{40}O_6$	63.80	10.71	63.50	10.93
7: n-$C_{16}H_{33}OH$	**15**	33	−76	$C_{22}H_{44}O_6$	65.31	10.96	64.98	11.18
8: n-$C_{18}H_{37}OH$	**16**	32	−70	$C_{24}H_{48}O_6$	66.13	11.18	66.23	11.42

Table 2 ^{13}C NMR data[a] (δ/ppm) of compounds **10**–**16**

Product	C-1	C-2	C-3[b]	C-4	C-5[b]	C-6	OCH_2CH_2	OCH_2CH_2	CH_3
10	62.4	100.6	69.5	70.5	69.5	64.2	60.9	31.9	14.3
11	64.4	102.2	71.7	72.3	71.7	65.8	62.7	33.6	15.1
12	64.0	102.1	71.1	72.0	71.6	65.7	62.4	33.6	14.5
13	62.0	100.1	69.1	70.1	69.6	63.6	60.4	31.6	13.0
14	63.8	101.9	70.9	71.8	71.4	65.5	62.2	33.4	15.2
15[c]	63.4	101.6	70.6	71.6	71.1	65.2	61.9	33.1	14.4
16[c]	63.5	101.6	70.6	71.6	71.1	65.2	61.9	33.1	14.4

[a] Spectra were recorded in CD_3OD. [b] Signals may be interchanged. [c] Spectrum was recorded in DMSO-d_6.

Table 3 ^1H NMR data[a] (δ/ppm; J/Hz) of compounds **10**–**16**

Compound	H-1	H-1′	H-3	H-4	H-5	H-6	H-6′	OCH_2	CH_3	$J_{H3\text{-}H4}$
10	3.72	3.74	3.94	3.71–3.82	3.66–3.87	3.68	3.71–3.82	3.48–3.57	0.94	9.90
11	3.59	3.62	3.81	3.63–3.69	3.71–3.74	3.56	3.63–3.69	3.42–3.48	0.80	9.90
12	3.71	3.74	3.92	3.75–3.80	3.85–3.86	3.66	3.75–3.80	3.46–3.55	0.85	10.0
13	3.69	3.74	3.91	3.73–3.79	3.83–3.84	3.65	3.73–3.79	3.45–3.54	0.90	9.8
14	3.68	3.74	3.90	3.73–3.78	3.82–3.83	3.64	3.73–3.78	3.44–3.53	0.89	9.9
15[b]	3.69	3.74	3.90	3.74–3.78	3.83–3.84	3.64	3.74–3.78	3.44–3.54	0.89	10.2
16[b]	3.69	3.74	3.91	3.73–3.80	3.83–3.84	3.64	3.73–3.80	3.50–3.60	0.90	10.2

[a] Spectra were recorded in CD_3OD. [b] Spectrum was recorded in DMSO-d_6.

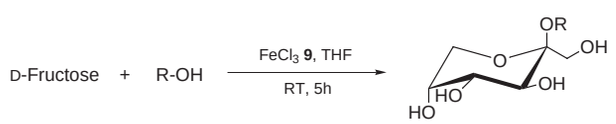

Scheme 1 Synthesis of alkyl β-D-fructopyranosides.

2 Synthesis of materials

A method for synthesizing alkyl glycosides from totally unprotected carbohydrates requires (i) control of tautomeric equilibria, especially when starting from D-fructose **1**, (ii) glycosidic linkage formation between the donor and the alkyl acceptor which is faster than the self-condensation of the sugar and (iii) stereocontrol of the anomeric configuration of the product. In addition, in order to avoid oligomerization of fructose, the reactions were performed in heterogeneous media.

Long chain alcohols **2**–**8** (see Scheme 1) are highly soluble in dichloromethane, acetonitrile or tetrahydrofuran (THF), while D-fructose is not, the former were therefore employed in a large excess with respect to the latter. After experimentation, the best results were found to be achieved when D-fructose (1 equiv.) was suspended in THF in the presence of an acceptor **2**–**8** (1.5 equiv.) and ferric chloride, **9**, (3 equiv.) as the promoter.[23] After 5 h at room temperature, alkyl β-D-fructopyranosides, **10**–**16**, with hydrocarbon chains carrying an even number of carbon atoms (varying between C_6 and C_{18}), were obtained in 30–35% yield (see Scheme 1). The formation of other isomers was not observed under the conditions described, and furthermore neither 5-hydroxymethylfurfural nor difructose dianhydrides were isolated in any significant quantities even after *in situ* acetylation.[24a]

The moderate yields can be explained by the high affinity of D-fructose for iron(III) cations.[25] Indeed, the complexation phenomena probably tend to decrease the acidity of the promoter and thus its ability to activate the anomeric centre.[24] In addition, the strong interaction between D-fructose and iron(III) cations could also be responsible for the diastereocontrol which results in the stereospecific formation of the β-D-fructopyranosides.

The structures of the amphiphiles synthesized, **10**–**16**, were deduced from the determination of their specific rotations (see Table 1) and from NMR spectroscopic data (see Tables 2 and 3). Measurements of their optical activity afforded values between −70° and −111° which are related to the presence of the β-pyranose form.[17b] The data obtained for the specific rotations correlate well with the ^{13}C NMR findings since the C-2 anomeric centre resonates approximately at 101 ppm, *i.e.*, at a lower field than that observed for the alkyl fructofuranosides.[20b] Confirmation of the presence of the pyranose form was achieved from the study of J coupling values obtained from the ^1H NMR spectra. Since the anomeric proton is absent, structural confirmation relied upon the coupling pattern between H-3 and H-4 (Table 3), and the large $J_{3,4}$ value (10 Hz), which unequivocally indicated a $^2C_5$ conformation.

Thus, a method for the diastereospecific synthesis of alkyl β-D-fructopyranosides has been demonstrated. The anomeric configuration imposes a fixed $^2C_5$ conformation in which the hydrophobic domain of the alkyl chain is extended to the hydrophilic sugar head, creating a facial amphiphilicity for compounds **10**–**16**.

General experimental methods

Melting points were determined using a Reichert hot-plate microscope and are uncorrected. Optical rotations were measured with a Perkin-Elmer polarimeter 341. ^{1}H, ^{13}C NMR spectra, at 400 and 100 MHz, respectively, and HETCOR and COSY NMR spectra were recorded using a Brüker ARX 400 spectrometer employing tetramethylsilane as an internal standard. Elemental analyses were produced by the Service de Microanalyse de l'ENSCR (France). Thin layer chromatography (TLC) analyses were conducted on Merck $60F_{254}$ silica gel non-activated plates and the compounds were visualised using a 5% solution of H_2SO_4 in ethanol. For column chromatography, Merck 60H (5–40 μm) silica gel was used. All reagents were purchased from either Acros or Aldrich Chemical Co. Tetrahydrofuran (THF) was dried by distillation from sodium.

General synthetic procedure

To a suspension of D-fructose (20 mmol, 3.60 g) in THF (30 ml), cooled to 0 °C, was added the appropriate alcohol (30 mmol). Ferric chloride (60 mmol, 9.72 g) was then added in small amounts. After stirring at room temperature for 5 h, the reaction mixture was diluted with ethyl acetate (100 ml) and washed with a 5% aq. HCl solution until it became decoloured. The aqueous layers were then extracted with ethyl acetate (3 × 20 ml), and the combined organic layers were washed with water (3 × 15 ml). The solvent was directly removed under reduced pressure, *without drying over $MgSO_4$*, and the resulting residue was purified by column chromatography using CH_2Cl_2–MeOH (95/5) as the eluent. Yields and analytical data for the alkyl β-D-fructopyranosides **10**–**16** are given in Tables 1–3.

3 Characterisation of materials

General experimental procedures

Phase identifications and the determination of phase transition temperatures were carried out by thermal polarised light microscopy using either a Zeiss Universal or a Leitz Laborlux 12 Pol polarizing transmitted light microscope equipped with a Mettler FP82 microfurnace in conjunction with an FP80 Central Processor. Sample preparations suitable for phase characterisations were prepared simply by using cleaned glass microscope slides or by using nylon coated slides. Nylon coating of the slides (~200–300 Å thick) was achieved by dipping clean slides into a solution of nylon (6/6) in formic acid (1% wt/vol). The nylon solution was allowed to drain off the slides over a period of 1 h, and then the slides were baked dry, free from solvent, in an oven at 100 °C for a period of 3 h. The slides were not buffed, as is usual for preparing aligned samples of liquid crystals, but instead they were used untreated so that many defects would be created when the mesomorphic state formed on the surface of the slide on cooling from the isotropic liquid.

Differential scanning calorimetry was used to confirm the phase transition temperatures determined by optical microscopy. Differential scanning thermograms (scan rate 1, 5 and 10° min^{-1}) were obtained using a Perkin-Elmer DSC 7 PC system operating on UNIX software. The results obtained were standardised relative to indium (measured onset 156.7 °C, ΔH 28.5 J g^{-1}, literature value 156.6 °C, ΔH 28.45 J g^{-1}).[26] Comparison of the transition temperatures determined by optical microscopy and differential scanning calorimetry shows some slight discrepancies. This is due to two factors; firstly, the two methods used separate instruments which are calibrated in different ways, and secondly, and more importantly, the carbohydrates tended to decompose slightly at elevated temperatures and at different rates depending on the rate of heating, the time spent at an elevated temperature and the nature of the supporting substrate, *i.e.*, the materials decomposed more quickly in aluminium DSC pans than on glass microscope slides.

Classification of the mesophases of the products was attempted *via* binary phase diagrams which were constructed by determining the phase transition temperatures of individual binary mixtures of a test material mixed with the standard compound, *n*-octyl β-D-glucopyranoside, which exhibits an interdigitated smectic A* phase. The binary mixtures were produced by weighing out each individual test material and the known standard material on a microscope slide and mixing them thoroughly while in their liquid states. The cooled samples were introduced into the microscope microfurnace and the phase transition temperatures and classification of phase type were performed in the usual manner. Typically, when the test and standard materials were mixed on a microscope slide while in their liquid states, some decomposition occurred thereby resulting in transition temperatures that were lower than expected. In all cases, recrystallisation temperatures were not determined because the binary mixtures supercooled to room temperature in their liquid-crystalline states.

Molecular modelling studies were performed on a Silicon Graphics workstation (Indigo XS24, 4000) using the programs QUANTA and CHARMm. Within CHARMm, the Adopted Basis Newton Raphson (ABNR) algorithm was used to locate the molecular conformation with the lowest potential energy. The minimisation calculations were performed until the root mean square (rms) force reached 4.184 kJ mol^{-1} $Å^{-1}$, which is close to the resolution limit. The rms force is a direct measure of the tolerance applied to the energy gradient (*i.e.*, the rate of change of potential energy with step number) during each cycle of minimisation. The calculation was terminated in cases where the average energy gradient was less than the specified value. The results of the molecular mechanics calculations were generated using the programs QUANTA V 4.0 and CHARMm V22.2. The programs were developed and integrated by Molecular Simulations Inc. The modelling packages assume the molecules to be a collection of hard particles held together by elastic forces, in the gas phase at absolute zero in an ideal motionless state, and the force fields used are those described in CHARMm V 22.2.

The structures of the liquid crystal phases formed by the materials were also investigated by powder X-ray diffraction (XRD). Initial experiments were carried out using a Rigaku Rotaflex RU-300 18 kW rotating anode source. Cu-Kα radiation was used, giving an X-ray wavelength of 1.541 E. The resolution, parallel to the diffraction plane, determined by slits and a pyrolytic graphite monochromator, was $\Delta Q_{\|} = 1.4 \times 10^{-2}$ $Å^{-1}$ [full peak width at half maximum (FWHM)]. Scattering angles were measured using a Huber four circle diffractometer in conjunction with SPEC analytical software. Higher resolution experiments were carried out at the Brookhaven National Synchrotron Light Source (NSLS), beamline X16B. Using a sagitally focusing Ge (111) monochromator crystal, a resolution of $\Delta Q_{\|} = 1.3 \times 10^{-3}$ $Å^{-1}$ (FWHM) was achieved at an X-ray wavelength of 1.630 Å. Scattering angles were measured using a Huber four circle diffractometer in conjunction with ACE analytical software. In both XRD experiments, the material was contained in a thin walled Lindemann silica capillary with an inside diameter of *ca.* 1 mm. The samples were held in a one-stage oven modified to accept capillary samples and positioned at the centre of rotation of the diffractometer.

Transition temperatures

The clearing points determined by thermal polarizing optical microscopy and melting points measured by DSC on the first heating cycle are shown together in Table 4 as a function of the alkyl chain length (*n*).

It is interesting to note the appearance of a smectic A* phase for the dodecyl β-D-fructopyranoside, **13**, only to find its demise by the octadecyl analogue, **16**. Secondly, on cooling from the smectic A* phase for the C_{12}, C_{14} and C_{16} homologues, or the

Table 4 Transition temperature (°C) for the fructopyranosides as a function of alkyl chain length (*n*). X is an unidentified phase

Compound	Chain length (*n*)	Cryst.[a]		SmA*		X		Iso. Liq.
10	6	·	124.4	—	—	·	124.4	·
11	8	·	128.5	—	—	·	131.0	·
12	10	·	129.1	—	—	·	133.3	·
13	12	·	128.6	·	131.6	·	132.7	·
14	14	·	130.0	·	130.3	·	135.3	·
15	16	·	129.6	·	129.9	·	135.8	·
16	18	·	114.5	—	—	·	128.2	·

[a] Determined by DSC.

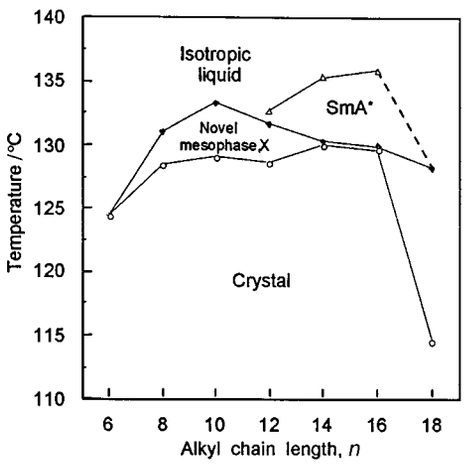

Fig. 2 Variation in transition temperatures and melting points as a function of the length of the alkyl substituent (*n*).

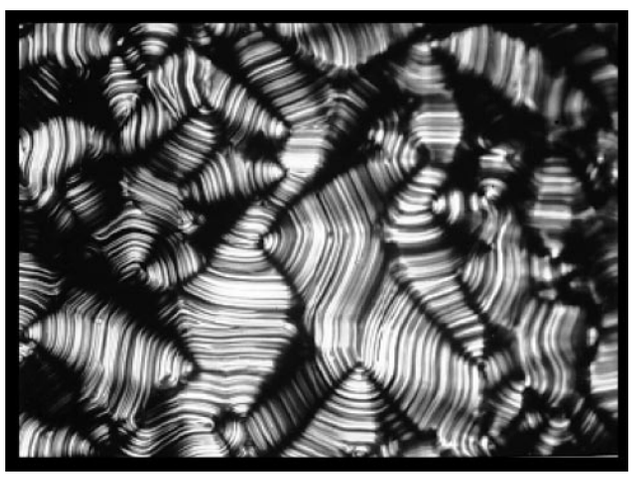

Fig. 3 Photomicrograph of the edge dislocation, with associated walls, texture of tetradecyl β-D-fructopyranoside in the X phase on an untreated substrate (×100).

isotropic liquid for the remaining compounds, a hitherto unobserved mesophase was found. The thermal stability of the new phase, X, initially increases with chain length only to marginally decrease from the decyl homologue onwards. Finally, the melting points do not seem to be affected much by the length of the alkyl substituent, with the exception of the C_{18} member. Fig. 2 depicts these property–structure correlations as a function of alkyl chain length.

Thermal optical microscopy

The mesophase formed directly from the isotropic liquid for the C_{12}, C_{14} and C_{16} homologues was classified as a smectic A* phase from observations of the defect textures exhibited by the mesophase on cooling from the isotropic liquid, and through miscibility studies with the standard material octyl β-D-glucopyranoside.

The defect textures exhibited by this mesophase fall into three categories. On untreated clean glass substrates focal-conic, oily streak and homeotropic defect textures were observed. On glass substrates coated with nylon, homogeneous alignment was achieved, and focal-conic defects, characterised by their elliptical and hyperbolic lines of optical discontinuity, were observed. The presence of focal-conic defects and homeotropic alignment in variously treated specimens is diagnostic for the presence of a smectic A phase. In addition, as the molecules are chiral, the specimens were examined for any indication of the formation of a helical macrostructure, *e.g.*, banding in the focal-conic domains, rotation of plane polarized light and selective reflection of light, however, none of these effects were found. Thus, the materials do not exhibit the twisted form of the smectic A phase, *i.e.* the twist grain boundary phase. These results classify the phase as being smectic A* in type; and miscibility studies with octyl β-D-glucopyranoside,[27] a standard carbohydrate exhibiting an SmA_d* phase, confirmed this classification of the liquid crystal phase. Moreover, mechanical disturbance of the material in this texture shows that the relative viscosity of the phase is low for a system which is extensively hydrogen bonded, which leads to the suggestion that the in-plane and out-of-plane positional ordering of the molecules is short range and the hydrogen bonding is dynamic.

All of the materials were found to exhibit the new phase, X, either by cooling from the isotropic liquid or from the smectic A* phase. Mesophase classification was attempted by examination of the defect textures observed on cooling from the preceding phase (smectic A* or isotropic liquid). Taking the tetradecyl homologue as an example, upon cooling from either the homeotropic or focal-conic smectic A* phase, worm-like filaments or ribbons slowly separated from the smectic A* regions and coalesced in the bulk to form a fan-like texture with a large number of what appear to be edge dislocations and their associated high energy walls in the vicinity of the defect cores. No hyperbolic or elliptical discontinuities[28,29] were observed indicating that the X-phase does not have a lamellar structure where the molecules are positionally disordered.

Fig. 3 shows a photomicrograph of the edge dislocations and associated walls for tetradecyl β-D-fructopyranoside produced using untreated slides. In addition, no surface treatment was capable of inducing a homeotropic texture for the X phase. Indeed in paramorphotic formation from the smectic A* phase, the destruction of the homeotropic texture at the transition to the X phase strongly suggests that the X phase is not lamellar in character.

The presence of the banded fan-like defects for the X phase indicates that it could have a columnar structure where the molecules are ordered along the column axes.[30–32] Fig. 4 shows a comparative photomicrograph and diagrammatic explanation for the formation of homogenous and fan-like defect textures in columnar mesophases formed by related materials. Apart from the lines shown across the backs of the fans in the defect texture of the X-phase shown in Fig. 3, the textures would be almost identical in character. In addition, the X phase was found to be difficult to shear, indicating that it has a much higher viscosity than the layered smectic A* phase. This shows that the X phase

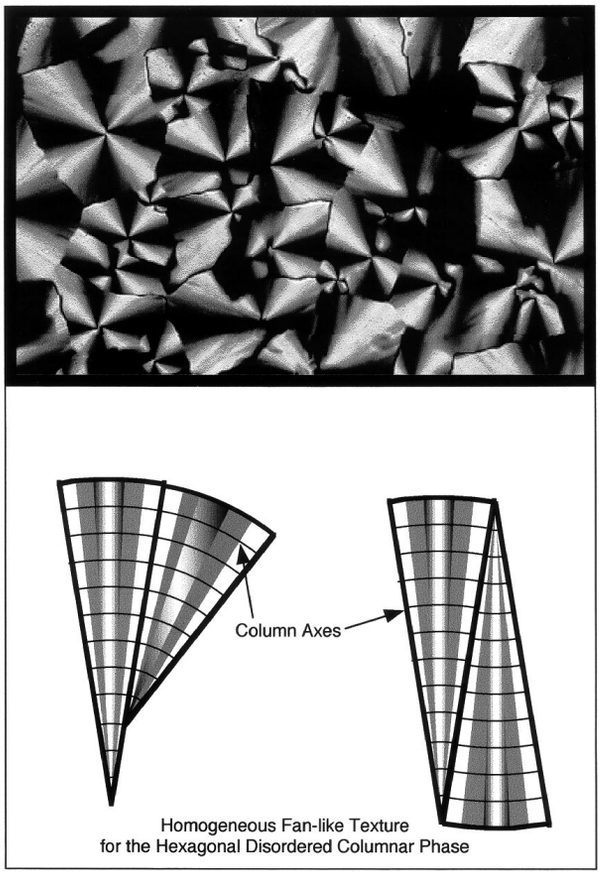

Fig. 4 A typical defect texture for the hexagonal disordered columnar phase.

has a more ordered structure, which agrees with the hypothesis that it is columnar in nature. Columnar mesophases generally have structures based on either rectangular or hexagonal packing of the columns. Hexagonal phases can exhibit both homeotropic and homogeneous textures, whereas the textures associated with a rectangular phase tend to be birefringent. Thus, if the X phase is columnar, the fact that homeotropic textures were not formed indicates that the columnar phase is most likely of the rectangular ordering type.

X-Ray diffraction studies

In order to explore the possibility of the new X phase being columnar instead of lamellar, as seems probable from the defect textures, we performed powder diffraction scans of the X-phase as well as the smectic A* phase. We can interpret the XRD results by referring to an orthogonal reciprocal lattice space in which the c^* axis is oriented parallel to the columnar axis. The 2D columnar ordering then results in (hk0) diffraction features in the a^*b^* plane. Moreover, to characterise the evolution in structure between the higher temperature smectic A* phase and the X phase, it is convenient to take the a^* axis as normal to the smectic A* layer planes (see Fig. 12). This choice of reciprocal lattice results in the smectic A* layer diffraction peaks being labelled as (h00) reflections rather than the more conventional label of (00l) reflections. Finally, as is quite common in lyotropic compounds, we can initially assume that the X phase columns are comprised of molecules radially oriented about a central core, and hence, the diameter of the columns is approximately equal to twice the molecular length. The spacing between the columns, however, could be considerably less than this diameter if the molecules interdigitate.

Fig. 5 shows a photomicrograph of the XRD pattern from a powder sample of tetradecyl β-D-fructopyranoside in the X phase at 127.6 °C using the rotating anode; the bright spot at the centre of the photomicrograph corresponds to the incident

Table 5 Summary of the powder XRD of tetradecyl β-D-fructopyranoside in the X phase at 127.6 °C

Reflection	2θ angle/°	d/Å
(100)	2.9513	29.94
(110)	not seen	not seen
(200)	5.96	14.8
unassigned	14.83	6.0
unassigned	17.7	5.0

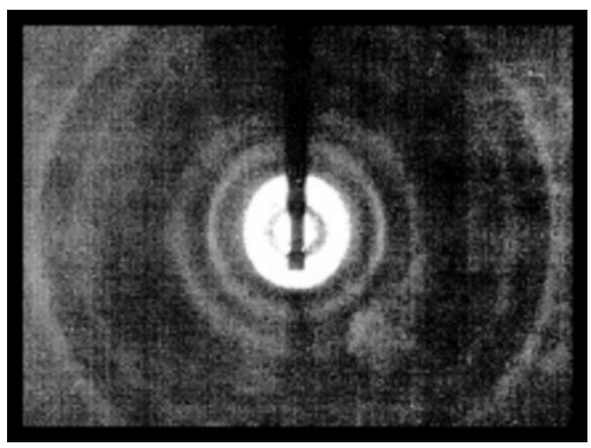

Fig. 5 Photomicrograph of the XRD pattern from a powder sample of tetradecyl β-D-fructopyranoside in the X phase at 127.6 °C. Incident power = 50 kV × 200 mA, no attenuation. Iso 3000/36° Polaroid film, positioned normal to the incident beam and 10.7 cm from the centre of rotation, 150 minute exposure time. The dark vertical line is the shadow of the beam stop and full diffraction circles could not be obtained for angles greater than 15° due to the 30° X-ray access allowed by the oven's windows.

beam. The diffraction angles of the various reflections were subsequently measured using a point detector attached to the 2θ circle of the diffractometer and are reported in Table 5. The third reflection from the centre (2$\theta \approx 7.9°$) is not tabulated because it was shown, *via* a placebo run, to be due to scattering from the oven's Kapton windows. In the small angle region, two reflections were observed that we label (100) and (200) since $Q_{\|}$ (200) = 2$Q_{\|}$ (100). There was no evidence for an additional diffraction feature between these two reflections.

From energy minimisation calculations using QUANTA and CHARMm, the diameter of the sugar moiety of tetradecyl β-D-fructopyranoside was estimated to be *ca.* 6.2 Å, its thickness *ca.* 4.0 Å and the overall molecular length with an all *trans* alkyl chain *ca.* 21.9 Å. Hence, the two large angle reflections giving distances of 5.0 and 6.0 Å can be ascribed to distances between adjacent carbohydrate moieties. The fact that scattering occurs at these large angles strongly suggests that the mesophase under investigation, whether columnar or not, is highly ordered in relation to the smectic A* phase where there is no in-plane order of the molecules and the layers are essentially liquid-like. Additionally, if we assume that the molecules interdigitate, then the (100) assignment of the peak at 29.94 Å (1.37 × the all *trans* molecular length) is consistent with a close packing of the columns. On the other hand, the X-ray photomicrograph shown in Fig. 5 lacks a (110) reflection. In the 17 possible 2D space groups, for which the (100) and (200) are allowed reflections, the (110) reflection is also allowed. For example, a hexagonal 2D space group would have a (110) reflection with associated wavevector $Q_{\|}$ (110) = $\sqrt{3}$ $Q_{\|}$ (100) = 1.73 $Q_{\|}$ (100). Similarly, a square 2D space group would have a (110) reflection with associated wavevector $Q_{\|}$ (110) = $\sqrt{2}$ $Q_{\|}$ (100) = 1.41 $Q_{\|}$ (100). The convolution of the columnar form factor with the structure factor results in a reduction in diffracted intensity at higher angles. The intensity of higher order peaks could also be decreased due to thermal vibrations or lattice

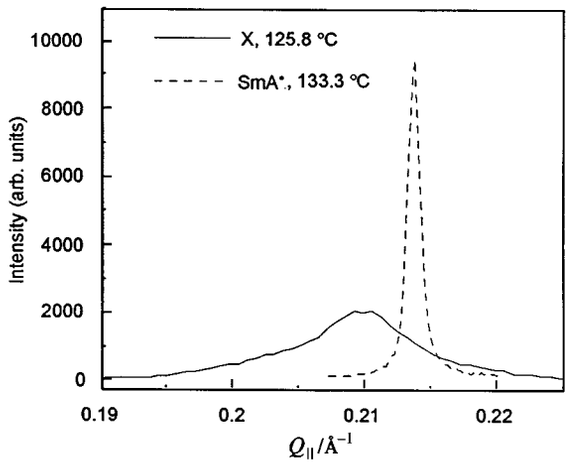

Fig. 6 Primary reflections of tetradecyl β-D-fructopyranoside at 133.3 and 125.8 °C. Notice the increase in FWHM in the X phase.

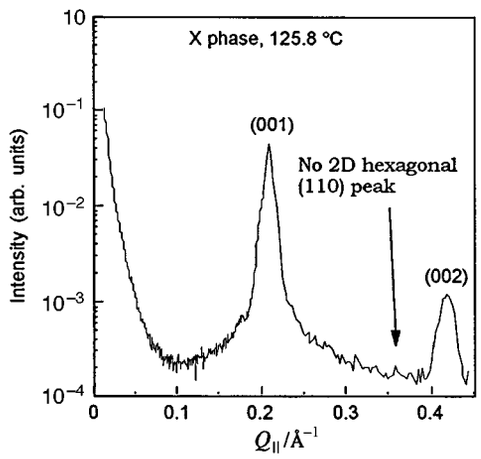

Fig. 7 Low angle scan in $Q_{\|}$ space of tetradecyl β-D-fructopyranoside at 125.8 °C in the X phase.

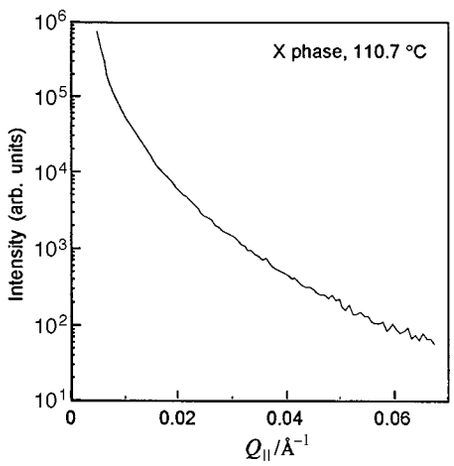

Fig. 8 Very low angle (down to 0.07°) scan in $Q_{\|}$ space of tetradecyl β-D-fructopyranoside at 110.7 °C in the X phase.

defects. If any of these factors were responsible for the absence of the (110) reflection, however, the (200) reflection (at even higher angle, and of the same order) would also vanish, and from Fig. 5, we see that it is clearly present. There is always the possibility that the columnar form factor has a zero that coincides with the location of the (110) reflection, and hence, we cannot definitively rule out that the X phase has a simple 2D packed structure. Nonetheless, the absence of the (110) reflection makes this structure highly unlikely.

Since the structural features needed to confirm a simple 2D columnar packing were absent in the moderate resolution XRD studies, more detailed structural investigations were made in order to try to resolve the quandary. Two possible ways of elucidating the situation were to orient the sample or to increase the beam resolution and intensity in the XRD experiments. Numerous methods to align and orient the liquid crystal material were attempted but all were unsuccessful. The first and most obvious method was to spread a freely suspended film of tetradecyl β-D-fructopyranoside in the smectic A* phase and to cool (1 °C h^{-1}) the sample into the X mesophase. After substantial supercooling, of the order of 10 °C at such low cooling rates, the film ruptured upon transition to the lower temperature X phase. Alignment in a strong magnetic field (1 tesla, upon slow cooling from smectic A* phase) was also unsuccessful as the XRD pattern did not change qualitatively or quantitatively from the powder diffraction pattern described above. The third method used in an attempt to orient the phase was to cool the material into the novel mesophase sandwiched in a thin cell that had coated alignment surface layers, but again no alignment was achieved.

As we were unable to produce an aligned specimen for study we then turned to an alternative method which was to increase the resolution and intensity of the beam in the powder X-ray diffraction experiment by using beamline X16B at the Brookhaven NSLS. Evidence for the structure of the X phase was expected to be found in the low angle regions in reciprocal space, rather than in the higher angle regions which deal with the local arrangement of molecules within a macrostructure. Thus, Fig. 6 shows the (100) reflection of the tetradecyl analogue at 133.3 and 125.8 °C in the SmA* and the novel X mesophase respectively. The peak width in the smectic A* phase is effectively resolution limited (FWHM = 1.31×10^{-3} Å^{-1}), whereas the same reflection in the X phase is much wider at some 6 × resolution (FWHM = 8.3×10^{-3} Å^{-1}), indicating a short-range reflection plane order with a correlation length of *ca.* 230 Å (*ca.* 8 × smectic A* bilayers). The correlation length was estimated on the assumption that correlations decayed exponentially which is reasonable since the diffraction peaks have a Lorentzian shape. The short-range correlation length for the layer ordering supports the possibility of a composite columnar structure that retains local, finite-sized, smectic-A* regions as one of its structural components.

A $Q_{\|}$ scan at 125.8 °C in the X phase, shown in Fig. 7, confirms the absence of a (110) reflection as observed in the moderate resolution studies. This $Q_{\|}$ scan also shows that, like the (100) reflection, the (200) reflection is not resolution-limited. A logarithmic plot was used to emphasise small features. If we assume that the composite columnar structure is composed of layered sub-units, which are responsible for the observed broad (100) and (200) reflections, then there could exist additional diffraction features at lower $Q_{\|}$ wavevectors associated with a 2D ordering of these larger columnar sub-units. Fig. 8 shows a low angle scan which probed the existence of these lower $Q_{\|}$ wavevectors. A wavevector region down to 0.0047 Å^{-1}, corresponding to *ca.* 0.13 μm, was explored but no peaks were observed. This implies that if a 2D structure with a large unit cell exists, then the scattering is either weak or the unit cell has a size larger than 0.13 μm.

Figs. 9 and 10 summarise the synchrotron XRD studies; the two figures show the temperature dependence of the width of the deconvoluted (100) peak, and the *d* spacing, determined from the (100) peak position. The first order smectic A*–X transition is clear in the plot shown in Fig. 9, even when plotted on a logarithmic scale, where a strong decrease in correlation length is observed on lowering the temperature. Since the smectic A* phase peak width is resolution limited, the values plotted in Fig. 9 are artefacts of peak deconvolution and not a real measure of peak width.

In summary, the X-ray diffraction studies do not rule out the possibility of a columnar-type structure for the X phase,

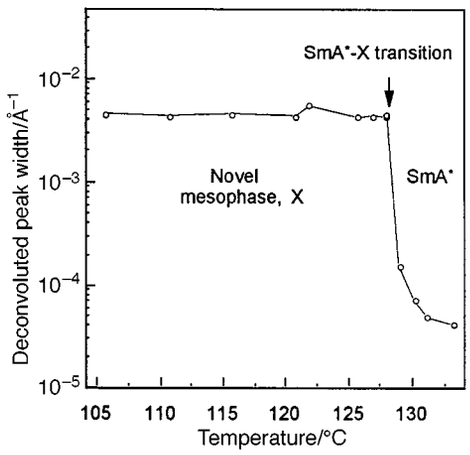

Fig. 9 Temperature dependence of the width of the deconvoluted primary $Q_{\|}$ peak.

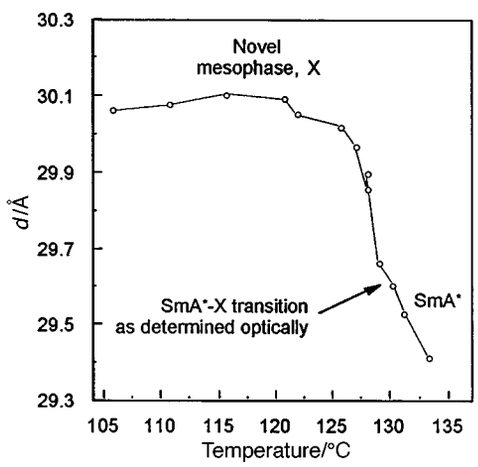

Fig. 10 Temperature dependence of the *d* spacing, determined from the (100) peak position.

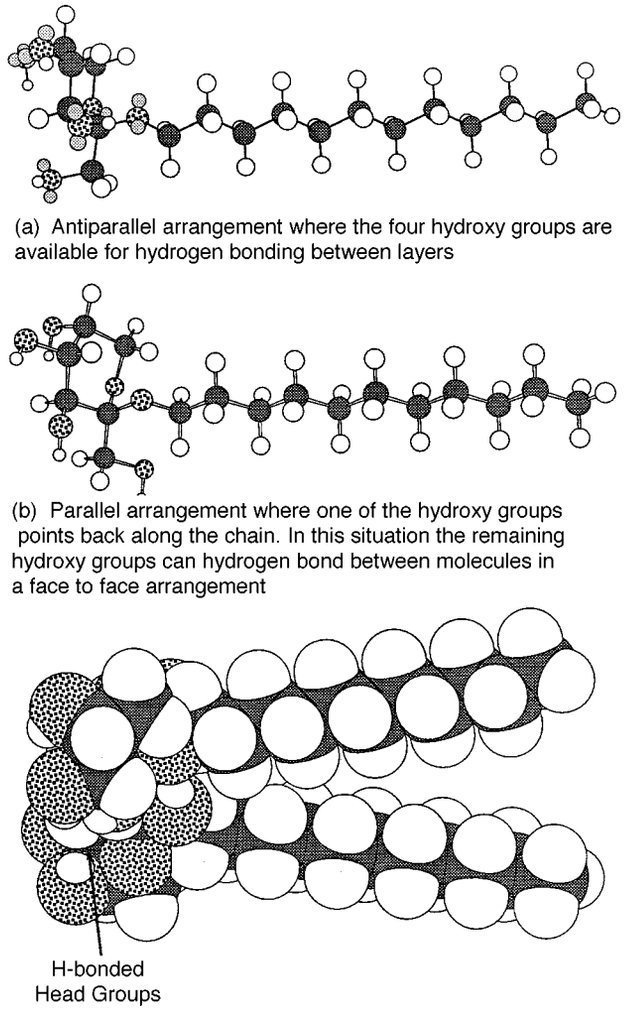

(a) Antiparallel arrangement where the four hydroxy groups are available for hydrogen bonding between layers

(b) Parallel arrangement where one of the hydroxy groups points back along the chain. In this situation the remaining hydroxy groups can hydrogen bond between molecules in a face to face arrangement

(c) Face to face hydrogen bonding creates wedge-shaped molecular pairs which can aid curvature

Fig. 11

although one would expect to see higher order reflections as well as those due to the (100) planes.[33] If the X-phase is columnar, however, the columns cannot be arranged in a simple 2D lattice, unless the dimensions of the lattice are extremely large. This suggests that if a columnar structure is present, then the columns will be packed in a disordered way. Alternatively, it is possible that the X phase is a viscous stratified phase with a structure which is not too far removed from that of the smectic A* phase, however, it would have to have the added feature of fewer defined reflection planes. On the other hand, optical microscopy investigations rule out the possibility that the X phase has a structure associated with any of the conventional disordered smectic lamellar phases. The formation of a fan-like defect texture at the expense of the development of a paramorphotic texture derived from the smectic A* phase suggests that the X phase has a columnar structure rather than a lamellar one. Similarly the generation of the X phase through the coalescence of filaments is strongly indicative of the presence of a columnar or tubular myelin structure. The X-ray correlation length of approximately eight layers suggests that the phase might have a columnar or ribbon-like structure made up of a number of layers or concentric tubes of molecules.

Molecular modelling

Modelling shows that the locations of three of the four hydroxy groups in the fructopyranoside moiety lie all on one side of the head group, whereas the fourth hydroxy group can possibly lie either antiparallel or parallel to the aliphatic chain, as shown in Fig. 11(a) and (b) respectively. For the antiparallel arrangement all four of the hydroxy groups are available for intermolecular hydrogen bonding which occurs between the layers of the molecules. For the parallel arrangement the hydrogen bonding takes place most easily between two facing molecules, but because of the locations of the hydroxy groups, the hydrogen bonding network cannot extend much further to other neighbouring molecules. This particular molecular pairing would lead to the formation of wedge shaped entities that would ultimately lead to negative curvatures or splay being introduced into the structure of the mesophase, see Fig. 11(c). These wedge-shaped structures would most likely be located along the inner bends of the bilayer structure. Here they would nucleate splaying of the layers thereby aiding the formation of edge dislocations. Interactions for the antiparallel arrangement of the hydroxy groups, the side-by-side arrangement of the molecules in layers can actually lead to wedge-shaped structures where the curvature would support positive bending of the layers. The combination of positive and negative curvature would therefore support bending of the layers and thereby formation of ribbons, columns or tubes. Consequently, a structure for the X phase made up of extended lamellae, as in a smectic phase, is unlikely if wedge-shaped molecular pairs are introduced into the layered structure.

In lyotropic systems, it is well known that the curvature introduced *via* differences in the size of the head group relative to the cross-sectional area of the lipophilic chain varies with solvent concentration. Curvature introduced *via* the packing of wedge- or conical-shaped molecules together strongly influences mesophase stability, with positive and negative curvatures at

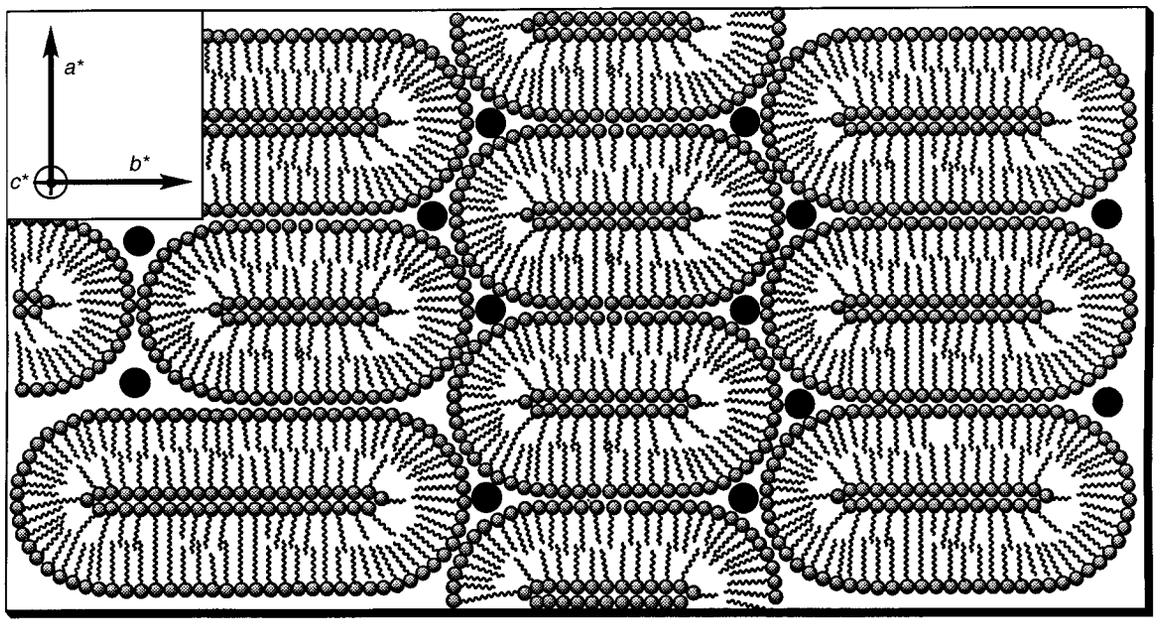

Fig. 12 Possible structure for the novel X phase. The locations of edge defects and walls are shown as black dots. For clarity the molecules in the figure are shown to be relatively well-ordered, but in the proposed mesophase they will be comparatively disordered.

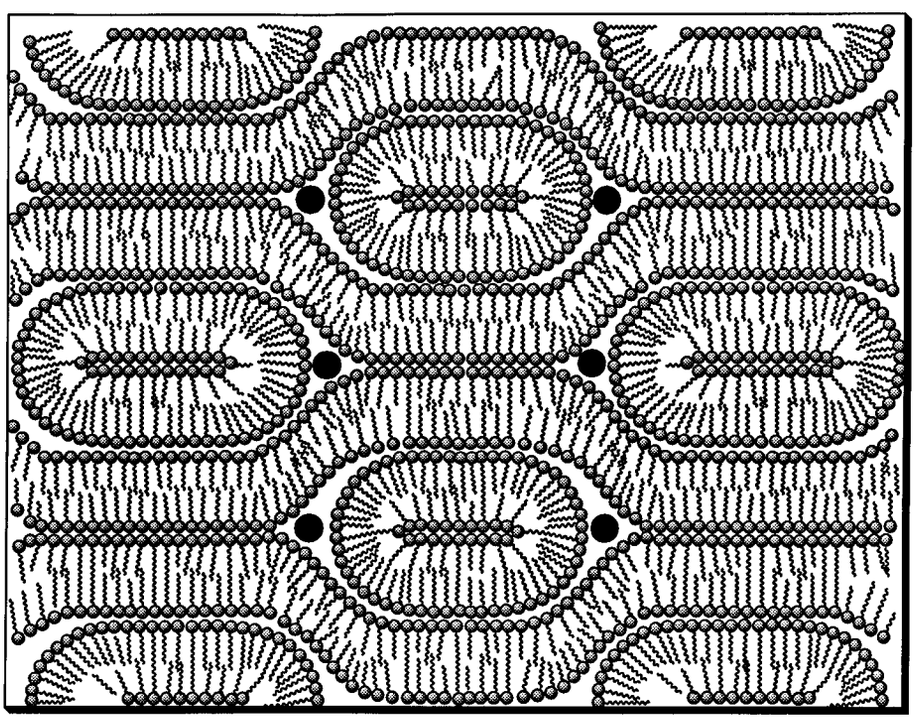

Fig. 13 A possible structural model for the X phase showing a combination of lamellar and columnar structures. The edge dislocations are shown as black dots. For clarity the molecules in the figure are shown to be relatively well-ordered, but in the proposed mesophase they will be comparatively disordered.

the concentration extremes and a lamellar arrangement with zero curvature in between.[34] In a similar way, on cooling from the smectic A* phase, one might anticipate an increase in curvature at the phase transition to the X phase due to the inclusion of wedge-shaped molecular pairs. Thus, it is possible that one of a number of structures based on a flattened columnar or ribbon model shown in Fig. 12 are possible. In this structure the basic form of the lamellar structure is retained, however, curvature is introduced *via* the introduction of edge dislocations. Thus a columnar-like structure is generated and some features of a lamellar structure are retained. Complex variations become possible when structures based on concentric layers, or mixtures of lamellar and columnar structures (Fig. 13) are considered. Such structures are not only in agreement with the increase in FWHM of the primary reflection but also the lack of higher order reflections and the proliferation of edge dislocations and associated walls seen in the defect texture shown in Fig. 3. Indeed, edge dislocations[35] are an intrinsic part of the layered mesophase as it is described earlier.

Similar arrangements have been observed in lyotropic systems[36] but, to the best of our knowledge, these structures have not been reported to date for thermotropic liquid-crystalline materials and we therefore tentatively put forward the ribbon-like ordering as the basis for a structure of the novel X phase. However, we would like to emphasise that we have no concrete evidence for this, only experimental agreement with our speculations. In addition to the ongoing alignment work, freeze fracture experiments, which were very successful in determining the

structure of the TGBA* phase,[37] are currently contemplated in order to describe the structure of the X phase.[38]

Conclusions

The novel synthesis and the investigation of the thermotropic liquid-crystalline self-organised properties of a family of *n*-alkyl β-D-fructopyranosides have been described in detail. The materials exhibit a novel mesophase, however, its structure remains an enigma at this time. Model structures that fit the X-ray data so far obtained were postulated, pending further investigations into the exact nature of the X phase. It is hoped that additional relationships between structure and the resulting molecular interactions may be drawn.

Acknowledgements

We thank the following agencies for their financial support; EPSRC and the Alliance Programme of the British Council and the Ministere des Affaires Etrangeres, Direction de la Cooperation Scientifique et Technique, the CNRS and the MENRT. We also thank ARD (Pomacle, France) for a grant to V. F.

References

1 B. Lindberg, *Adv. Carbohydr. Chem. Biochem.*, 1990, **48**, 279.
2 M. A. Clarke, A. V. Bailey, E. J. Roberts and W. S. Tsang, *Carbohydrates as Organic Raw Materials*, VCH, Ed. F. W. Lichtenthaler, 1991, pp. 169 and references therein.
3 (*a*) K. Bock, M. Meldal, B. Mayer and L. Wiebe, *Acta Chem. Scand. Ser. B*, 1983, **37**, 101; (*b*) P. J. Card, W. D. Hitz and K. G. Ripp, *J. Am. Chem. Soc.*, 1986, **108**, 158.
4 A. J. J. Straathof, J. P. Vrijenhoef, E. P. A. T. Sprangers, H. Van Bekkum and A. P. G. Kieboom, *J. Carbohydr. Chem.*, 1988, **7**, 223.
5 W. W. Binkley and M. L. Wolfrom, *J. Am. Chem. Soc.*, 1946, **68**, 2171.
6 (*a*) P. Birgl and R. Schinke, *Ber. Dtsch. Chem. Ges.*, 1934, **67**, 127; (*b*) J. W. van Cleve, *Methods Carbohydr. Chem.*, 1963, **2**, 237.
7 A. Bouali, G. Descotes, D. F. Ewing, A. Grouiller, J. Lefkidou, A. D. Lespinasse and G. Mackenzie, *J. Carbohydr. Chem.*, 1992, **11**, 159.
8 (*a*) L. V. Backinovsky, N. F. Balan, V. I. Betaneli and N. K. Kotchetkov, *Carbohydr. Res.*, 1982, **99**, 189; (*b*) N. F. Balan, L. V. Backinovsky, V. I. Betaneli and N. K. Kotchetkov, *Bioorg. Khim.*, 1981, **7**, 1566.
9 Y. L. Li and Y. L. Wu, *Tetrahedron Lett.*, 1996, **37**, 7413.
10 C. Krog-Jensen and S. Oscarson, *J. Org. Chem.*, 1996, **61**, 1234.
11 (*a*) F. Barresi and O. Hindsgaul, *J. Am. Chem. Soc.*, 1991, **113**, 9376; (*b*) K. Stork and J. Kim, *J. Am. Chem. Soc.*, 1992, **114**, 1087.
12 C. Krog-Jensen and S. Oscarson, *J. Org. Chem.*, 1996, **61**, 4512.
13 T. Müller, R. Schneider and R. R. Schmidt, *Tetrahedron Lett.*, 1994, **35**, 4763.
14 A. Haudréchy and P. Sinay, *Tetrahedron Lett.*, 1990, **31**, 5765.
15 F. Nicotra, L. Panza and G. Russo, *Tetrahedron Lett.*, 1991, **32**, 4035.
16 (*a*) B. M. Heskamp, G. H. Veeneman, G. A. van der Marel, C. A. A. van Boeckel and J. H. van Boom, *Tetrahedron*, 1995, **51**, 5657; (*b*) B. M. Heskamp, D. Noort, G. A. van der Marel and J. H. van Boom, *Synlett*, 1992, 713.
17 (*a*) F. W. Lichtenthaler, E. Cuny, D. Martin, S. Rönninger and T. Weber, *Carbohydrates as Organic Raw Materials*, VCH, Ed. F. W. Lichtenthaler, 1991, pp. 207; (*b*) B. Schneider, F. W. Lichtenthaler, G. Steinke and H. Schiweck, *Liebigs Ann. Chem.*, 1985, 2443.
18 W. Funke and A. Kremer, *Carbohydr. Res.*, 1976, **50**, 9.
19 E. Fischer, *Ber. Dtsch. Chem. Ges.*, 1893, **26**, 2406.
20 (*a*) C. P. Barry and J. Honeyman, *Adv. Carbohydr. Chem.*, 1952, **7**, 53; (*b*) Y. Haraguchi, A. Yagi, A. Koda, N. Inagashi, K. Noda and I. Nishioka, *J. Med. Chem.*, 1982, **25**, 1495.
21 (*a*) J. N. Bertho, V. Ferrières and D. Plusquellec, *J. Chem. Soc., Chem. Commun.*, 1995, 1391; (*b*) V. Ferrières, J. N. Bertho and D. Plusquellec, *Tetrahedron Lett.*, 1995, **36**, 2749.
22 D. Plusquellec, G. Chevalier, R. Talibart and H. Wróblewsky, *Anal. Biochem.*, 1989, **179**, 145 and references therein.
23 V. Ferrières, J. N. Bertho and D. Plusquellec, *Carbohydr. Res.*, 1998, **311**, 15.
24 (*a*) R. Velty, T. Benvegnu and D. Plusquellec, *Synlett*, 1996, 817; (*b*) R. Velty, T. Benvegnu, M. Gelin, E. Privat and D. Plusquellec, *Carbohydr. Res.*, 1997, **299**, 7.
25 K. Kruger and L. Nagy, *Biocoordination Chemistry*, Simon and Schuster, 1990, pp. 236.
26 CRC Handbook of Physics and Chemistry, 1988, ed. R. C. Priest, CRC Press, Boca Raton, 68th Edition.
27 J. W. Goodby, *Mol. Cryst. Liq. Cryst.*, 1984, **110**, 205.
28 G. Friedel, *Ann. Phys.*, 1922, **18**, 273.
29 G. W. Gray and J. W. Goodby, in *Smectic Liquid Crystals: Textures and Structures*, Leonard Hill, Philadelphia, 1984.
30 Y. Bouligand, *J. Phys.* (*Paris*), 1980, **41**, 1297.
31 Y. Bouligand, *J. Phys.* (*Paris*), 1980, **41**, 1307.
32 S. Chandrasekhar and G. S. Ranganath, *Recent Prog. Phys.*, 1990, **53**, 57.
33 H. Zheng, C. K. Lai and T. M. Swager, *Chem. Mater.*, 1995, **7**, 2067.
34 R. G. Laughlin, in *The Aqueous Phase Behaviour of Surfactants*, Academic Press, London, 1994.
35 P. G. de Gennes and J. Prost, in *The Physics of Liquid Crystals*, Oxford University Press, Oxford, 1993.
36 G. H. Brown and J. J. Wolken, in *Liquid Crystals and Biological Structures*, Academic Press, New York, 1979, p. 63.
37 K. J. Ihn, J. A. N. Zasadzinski, R. Pindak, A. J. Slaney and J. W. Goodby, *Science*, 1992, **258**, 275.
38 R. Pindak, personal communication.

Paper 9/00192A